Journal of Controlled Release 330 (2021) 362–371

Contents lists available at ScienceDirect

Journal of Controlled Release

journal homepage: www.elsevier.com/locate/jconrel

Albumin-binding prodrugs *via* reversible iminoboronate forming nanoparticles for cancer drug delivery

Lingqiao Hao [a,1], Quan Zhou [a,1], Ying Piao [a,b], Zhuxian Zhou [a,b], Jianbin Tang [a], Youqing Shen [a,b,*]

[a] Center for Bionanoengineering and Key Laboratory of Biomass Chemical Engineering of Ministry of Education, College of Chemical and Biological Engineering, Zhejiang University, Zheda Road 38, Hangzhou 310007, China
[b] ZJU-Hangzhou Global Scientific and Technological Innovation Center, Hangzhou, Zhejiang 311215, China

ARTICLE INFO

Keywords:
Albumin-based nanomedicine
Prodrug
Iminoboronate chemistry
Acid and GSH-responsive release
Camptothecin
Curcumin

ABSTRACT

Albumin-based nanomedicines are important nanoplatforms for cancer drug delivery. The drugs are either physically encapsulated or covalently conjugated to albumin or albumin-based nanosystems. Physical encapsulation is advantageous due to requiring no chemical modification of drug molecules, but many drugs, for instance, camptothecin (CPT) and curcumin (CCM), though very hydrophobic, can't be loaded in or form nanoformulations with albumin. Herein, we demonstrate prodrugs readily binding to proteins *via* iminoboronates and forming nanoparticles for cancer drug delivery. CPT and CCM were functionalized with 2-acetylphenylboronic acid (2-APBA) to produce prodrugs CPT-SS-APBA and CCM- APBA. The prodrugs bound to bovine serum albumin (BSA) *via* formation of iminoboronates and the produced BSA/prodrug readily self-assembled into well-defined nanoparticles with high loading efficiency, improved colloidal stability, and much-improved pharmacokinetics. The nanoparticles effectively released drugs in the intracellular acidic environment or the cytosol rich in glutathione (GSH). *In vivo*, the nanoparticles showed enhanced anticancer efficacy compared with clinically used irinotecan or sorafenib in subcutaneous 4 T1 or HepG2 tumor models. This work demonstrates a versatile protein-binding prodrug platform applicable to protein-based drug formulations and even antibody-drug conjugates.

1. Introduction

Albumin has been extensively explored as drug delivery carriers owing to its advantages, including high biocompatibility, non-antigenicity, good biodegradability, and easy surface modification [1–3]. To date, several albumin-based nanosized drug delivery systems have successfully clinical translated, which significantly improved the pharmacokinetics and tumor accumulation of therapeutics, and thus improved drugs' therapeutic efficiency and minimized side effects [2,4].

Albumin is inherently capable of hosting hydrophobic molecules in its hydrophobic interiors, and thus physical encapsulation of drugs is preferable due to avoiding chemical modifications [5,6]. Some albumin-based nanomedicines have already been approved for clinical use or in clinical trials [3,7,8]. A most successful example is Abraxane, a human albumin nanoparticle encapsulated with paclitaxel (PTX) approved by the FDA in 2005 and used widely in clinics for the first-line treatment of locally advanced or metastatic cancer [9]. It shows obvious clinical advantages over the first-generation Cremophor EL-based PTX (Taxol) [10]. Many hydrophobic anticancer drugs, however, cannot be loaded into albumin at acceptable drug loading contents. For example, physical encapsulation of very hydrophobic camptothecin (CPT) or curcumin (CCM) into the albumin or other proteins is still unsuccessful due to their intrinsically planar structure, moderate polarity, and extremely fast crystallization tendency [11,12]. Covalent conjugation is an alternative to load these drugs to albumin [13], including drug-albumin conjugate (MTX-HSA) [14] and albumin-binding prodrugs such as (6-maleimidocaproyl)hydrazone derivative of doxorubicin [15], monomethyl auristatin E [16]. The critical design is the intracellular cleavable linkers to release the carried drugs [17,18].

Iminoboronates have been extensively exploited to the biorthogonal

* Corresponding author at: Center for Bionanoengineering and Key Laboratory of Biomass Chemical Engineering of Ministry of Education, College of Chemical and Biological Engineering, Zhejiang University, Zheda Road 38, Hangzhou 310007, China.
E-mail address: shenyq@zju.edu.cn (Y. Shen).
[1] ǂEqual Contributors

https://doi.org/10.1016/j.jconrel.2020.12.035
Received 26 October 2020; Received in revised form 16 December 2020; Accepted 20 December 2020
Available online 24 December 2020

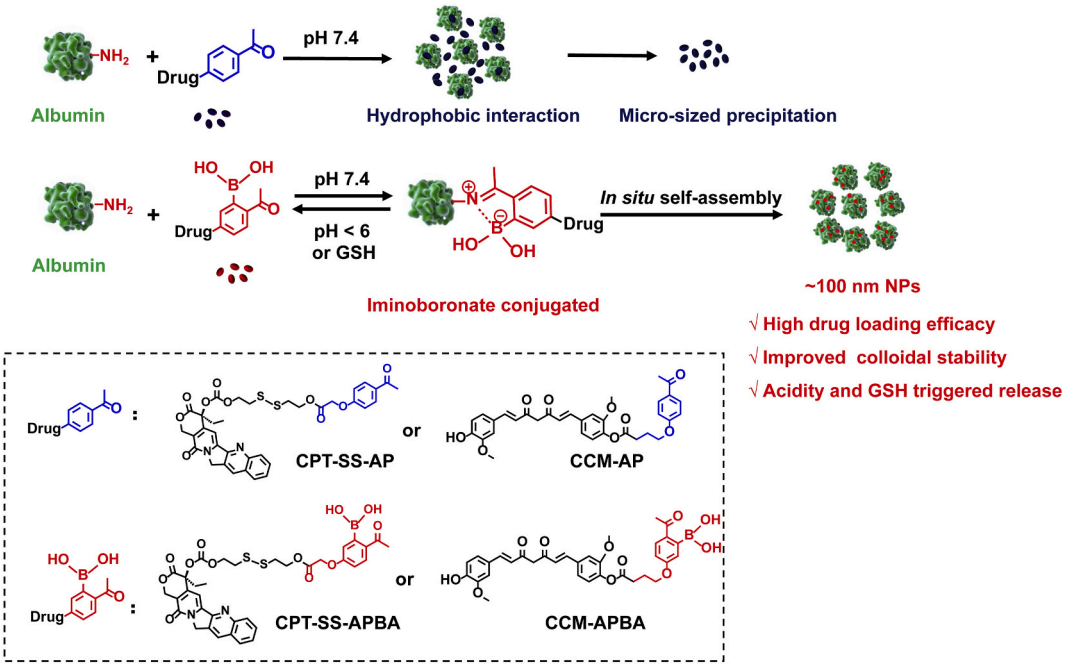

Scheme 1. Iminoboronate-forming prodrugs for BSA-binding. 2-Acetylphenylboronic acid (2-APBA) conjugated prodrugs (CPT-SS-APBA and CCM-APBA) rapidly bind to albumin *via* the iminoboronate. The hydrophobized BSA self-assembled into ~100 nm nanoparticles with high drug loading efficacy and improved colloidal stability. At the lysosomal pH or in the presence of GSH, the iminoboronate was quickly cleaved to release the drug. The control prodrugs with acetylphenyl (AP) group (CPT-SS-AP and CCM-AP) can't bind with BSA and the hydrophobic interactions among the free drug molecules dominate the self-assembly process to produce precipitates.

chemistry in recent years [19,20] as the reaction is regarded as a controllable and reversible "click reaction" and allows labeling biological amines at low millimolar concentrations with good thermodynamic stability [21,22]. Importantly, iminoboronates are very labile by acid or GSH due to cleavage of the B-N bond [23]. Thus, iminoboronates were used for efficient cyclization of peptides [24], reversible lysine modification [25], and cancer cell targeting [26].

Motivated by the formation of stable iminoboronates at pH of 6–9 between lysine ε-amino group and 2-acetylphenylboronic acid (2-APBA) [22], we herein demonstrate iminoboronate-forming prodrugs for *in-situ* albumin binding (Scheme 1). 2-APBA was conjugated to CPT or CCM (denoted as CPT-SS-APBA and CCM-APBA). We proposed that both CPT-SS-APBA and CCM-APBA readily bound to BSA *via* the iminoboronate chemistry and induced *in situ* self-assembly to form well-defined nanoparticles with high loading efficiency and improved colloidal stability. The loaded drugs are effectively unloaded in response to the lysosomal pH or intracellular GSH. As a result, the BSA/CPT-SS-APBA nanoparticles showed enhanced anticancer efficacy than the clinically used irinotecan (CPT-11) and sorafenib in subcutaneous 4 T1 and HepG2 tumor models. Apart from CPT and CCM, the current strategy may be extended to other hydrophobic drugs, rendering it a versatile and robust protein-binding prodrug platform applicable for protein-based drug formulations and even antibody-drug conjugates.

2. Materials and methods

2.1. Materials

All the materials other than indicated were purchased from Sinopharm Chemical Reagent Co., Ltd. (Shanghai, China). Dichloromethane (CH_2Cl_2, DCM), *N*,*N*-dimethylformamide (DMF), pyridine (Py), acetonitrile (MeCN), and triethylamine (TEA) were distilled over calcium hydride (CaH_2) or treated with a 4 Å molecular sieve to remove the residue water. Camptothecin (CPT) and irinotecan hydrochloride trihydrate (CPT-11) were purchased from Xindifu Pharmaceutical Co., Ltd. (Xi'an, China). Albumin, IgG, and RNase A were obtained from Sangon Biotech Co., Ltd. (Shanghai, China). The anti-PD1 antibody (aPD1) was purchased from Innovent Biologics Co., Ltd. (Suzhou, China). Curcumin was purchased from Energy Chemical Reagent Co., Ltd. (Shanghai, China). All the chemicals were used as received. Buffer solution (pH = 7.4) used here was prepared from Tris·HCl (0.1 M) and NaCl (15 mM).

2.2. Characterizations

^{1}H NMR, ^{13}C NMR, and ^{11}B NMR spectra were obtained on a 400 MHz Varian Gemini NMR spectrometer in deuterated solvents as noted. The sizes and zeta potentials of samples were measured at 25 °C on a Zetasizer Nano-ZS (Malvern Instruments, UK) with 632.8 nm laser light set at a scattering angle of 173°. HPLC analyses were performed using a Waters HPLC system consisting of a Waters 1525 binary pump, a Waters 2475 fluorescence detector, and a symmetry C18 column (5 μm, 4.6 × 250 mm Column) in a 1500 column heater. For detecting CPT, methyl alcohol-water (80:20) was used as the mobile phase at 35 °C at a flow rate of 1 mL/min. The fluorescence detector was set at 360 nm for excitation and 540 nm for emission. For detecting CCM and CCM-APBA, the mobile phase consists of acetonitrile and water (containing 0.1% TFA) in a gradient mode at a flow rate of 1 mL/min at 35 °C; the content of acetonitrile linearly increased from 50% to 80% within 30 min. The UV detection wavelength was set at 420 nm. Data were processed using Breeze software. Linear calibration curves for concentrations in the range of 0.001–10 μg/mL were constructed using the peak areas by linear regression analysis.

2.3. Preparation of BSA/CPT-SS-APBA nanoparticles

The preparation of BSA/CPT-SS-APBA nanoparticles ($m_{BSA}/m_{CPT\text{-}SS\text{-}APBA} = 5$) is as follows: CPT-SS-APBA (1 mg) was dissolved in 100 μL THF and added dropwise to 1 mL of BSA solution (5 mg/mL) with vigorous stirring. After stirring at r.t. for 10 min, THF was removed by rotary evaporator to give the BSA/CPT-SS-APBA solution. Other nanoparticles

were prepared in the same way, and the concentrations of RNase A, aPD1, and IgG were 2.5 mg/mL, 1 mg/mL, and 1 mg/mL, respectively. The *Z*-averaged diameters and zeta potentials of the prepared nanoparticles were determined by dynamic light scattering (DLS).

2.4. Stability assay of BSA/CPT-SS-APBA nanoparticles

The BSA/CPT-SS-APBA nanoparticles were incubated in 1640 cell culture medium (with 10% FBS) at 37 °C with shaking. The nanoparticle sizes and zeta-potentials were measured by DLS at different times.

2.5. Transmission Electron Microscope (TEM) observation

The prepared BSA/CPT-SS-APBA nanoparticle solution (CPT-SS-APBA equivalent concentration 0.5 mg/mL) was applied onto a 150-mesh carbon-copper grid. After wicking off the excess solution with filter paper, images were recorded using a transmission electron microscope (JEM-1200EX, TEM) operated at a voltage of 80 kV. For the lyophilized nanoparticles, the powder was redissolved in water (CPT-SS-APBA concentration, 0.5 mg/mL), and their sizes, zeta potentials, and morphology of the lyophilized nanoparticles were determined by DLS and TEM.

2.6. In vitro CPT release

Nanoparticle solution (CPT-SS-APBA equivalent concentration 1 mg/mL, 1 mL) was loaded into a dialysis bag (MWCO, 3.5 kDa) against 45 mL of PBS (pH 7.4 or 5.0) with or without 10 mM of GSH shaken at 37 °C at 200 rpm. At timed intervals, 0.1 mL of the PBS buffer solution was sampled and replaced with 0.1 mL fresh PBS buffer solution. After mixed with 0.9 mL acetonitrile, the released CPT content was measured by HPLC. Meanwhile, the particle sizes in the dialysis bag containing 10 mM GSH at pH 7.4 were detected using DLS at 0 h, 12 h, 24 h, and 48 h, respectively. The release kinetics of CCM from BSA/CCM-APBA nanoparticles at pH 7.4 or 5.0 were performed in the same way.

2.7. Cell lines and animals

All cell lines were obtained from the American Type Culture Collection (ATCC, Manassas, VA) and cultured in 1640 medium with 10% Fetal Bovine Serum (FBS, Gibco, Grand Island, USA), 1% penicillin/streptomycin (Sigma-Aldrich, St. Louis, USA).

Female BALB/c mice and ICR mice (6–8 weeks) were purchased from the Animal Center of Zhejiang University and maintained under standard conditions. Animal use and care were approved by the Animal Ethics Committee of Zhejiang University and were carried out in accordance with the institutional guidelines.

2.8. Cell viability assay

The cytotoxicity of BSA/CPT-SS-APBA nanoparticles (or BSA/CCM-APBA nanoparticles) to different cell lines was determined by the typical MTT (3-(4, 5-dimethyl-2-thiazolyl)-2, 5-diphenyl-2H-tetrazolium bromide) assay. In brief, cells were planted in 96-well plates with a density of 5000 cells per well and incubated for 24 h. The medium was replaced with a fresh medium containing the drugs at a series of designated concentrations. After 48 h incubation, 20 μL MTT (5 mg/mL) in PBS was added to each well, followed by incubation for another 4 h. Finally, the medium was carefully removed and replaced with 100 μL DMSO to dissolve the formazan crystals. The absorbance intensity of each well was measured in a Molecular Devices microplate reader at 562/620 nm. Each drug concentration was tested in triplicate and in three independent experiments.

2.9. In vivo pharmacokinetics

BSA/CPT-SS-APBA nanoparticles, CPT-SS-APBA dispersed in PEG400 (30%) or CPT-11 (5 mg CPT or SN38-eq./kg) were injected *via* the tail vein ($n = 3$ for each group). Blood samples (50 μL) were collected from the retro-orbital plexus of the mouse eye at timed intervals and then added with 0.1 N NaOH (50 μL). The mixtures were incubated at 37 °C overnight to release CPT or SN38 followed by adding with 1 mL of acetonitrile. The solution was sonicated and centrifuged at 5000 rpm for 5 min to obtain the supernatant, 200 μL of which was mixed with 200 μL 0.1 N HCl aqueous solution for HPLC analysis. The CPT or SN38 content was calculated according to the standard curve. Pharmacokinetic parameters were obtained using DAS by fitting a two-compartment model.

2.10. In vivo biodistribution

4 T1 tumor-bearing mice (tumor volume of ~200 mm^3) were intravenously injected with BSA/CPT-SS-APBA at 5 mg/kg CPT-equivalent (CPT-eq.) dose *via* the tail vein. Mice were sacrificed at 6 h after administration, and the tumor, heart, liver, spleen, lung, and kidney were collected. Weighted tissues were homogenized in 400 μL PBS and then added to 0.1 N NaOH (50 μL). The mixtures were incubated at 37 °C overnight followed by adding with 1 mL acetonitrile. The solution was sonicated and centrifuged at 5000 rpm for 5 min to obtain the supernatant, 200 μL of which was mixed with 200 μL 0.1 N HCl aqueous solution for HPLC analysis. The CPT content was calculated according to the standard curve.

2.11. In vivo antitumor activity

Subcutaneous 4 T1 tumor model: 4 T1 tumor-bearing mice (6–8 weeks old, female) were established by subcutaneous injection of a suspension of 5×10^5 4 T1 cells in PBS (100 μL). After 7 days post-inoculation, the mice were randomly divided into 3 groups ($n = 6$), and injected *via* the tail vein with 200 μL of PBS, CPT-11(5 mg/kg SN38-eq. dose) or BSA/CPT-SS-APBA (5 mg/kg CPT-eq. dose) for 6 times. Tumor volume and bodyweight of the mice were monitored every 2 days. When the tumor volume exceeded 1000 mm^3, mice were sacrificed, and the tumors were collected and weighed.

Subcutaneous HepG2 tumor model: HepG2 tumor-bearing nude mice (6–8 weeks old, female) were established by subcutaneous injection of a suspension of 4×10^6 HepG2 cells in PBS (100 μL). After 10 days post-inoculation, the mice were randomly divided into 3 groups ($n = 5$): PBS, sorafenib (oral administration of 10 mg/kg every two days for 6 times), and BSA/CPT-SS-APBA nanoparticles (intravenously administration of 5 mg/kg CPT-eq. dose every two days for 6 times). Tumor volume and mouse weight were monitored every 2 days. When the tumor volume exceeded 1000 mm^3, mice were sacrificed and the tumors were collected and weighed. Tumors and other organs were harvested and then fixed with 4% paraformaldehyde, embedded, sliced, and stained for H&E examination and TUNEL assay.

2.12. H&E staining

The freshly collected HepG2 tumor samples and some other organs (heart, liver, spleen, lung, and kidney) were washed in PBS, fixed with 4% neutral buffered paraformaldehyde, dehydrated by gradient concentration of ethanol and *p*-xylene, embedded in paraffin, and cross-sectioned at a thickness of 5 μm. The sections were stained with hematoxylin-eosin (H&E, Beyotime, China) and observed under light microscopy.

2.13. TUNEL immunofluorescence assay

The freshly collected subcutaneous HepG2 tumors were sectioned with a thickness of 4 μm, and the TUNEL immunofluorescence staining

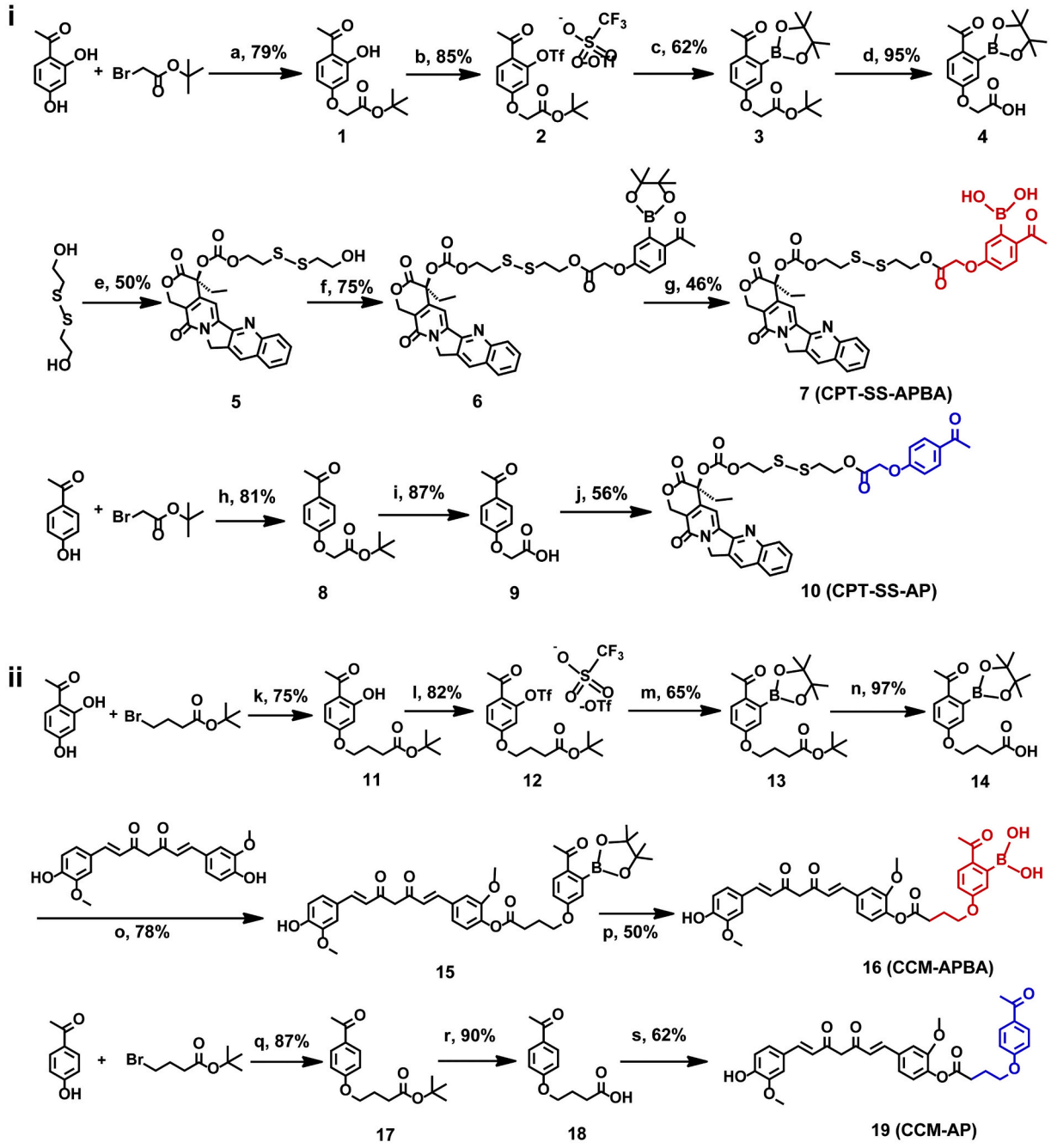

Scheme 2. Synthesis of 2-acetylphenylboronic acid (2-APBA) conjugated prodrugs and controls. *a,h*, *tert*-butyl bromoacetate, K_2CO_3, DMF, r.t., overnight; *b,l*, trifluoromethanesulfonic anhydride, pyridine, DCM, r.t., 24 h; *c,m*, bis(pinacolato)diboron, Pd(dppf)Cl_2dppf, potassium acetate, dioxane, 90 °C, 12 h; *d,i,n,r*, TFA, DCM, 6 h; *e*, CPT, triphosgene, 4-dimethylaminopyridine (DMAP), DCM/THF, r.t., 24 h; *f,j,o,s*, *N,N′*-dicyclohexylcarbodiimide(DCC)/DMAP, DCM, r.t., 24 h; *g,p*, boronic acid resin, CH_3CN: HCl (1 M) (9: 1), r.t., 24 h; *k,q*, *tert*-butyl 4-bromobutanoate, K_2CO_3, DMF, r.t., overnight.

was performed following the manufacturer's instructions. Briefly, the slices were fixed with cold acetone for 10 min, dried on slide rack for 30 min, rinsed with PBS (0.1 M, pH = 7.4) for 3 times, blocked with 10% goat serum for 60 min at r.t. and then incubated with the TUNEL antibody (Beyotime, 1:500) at 4 °C overnight. The sections were rinsed three times with PBS and further incubated with FAM-labeled second antibody (BD, 1:200) for 1 h at room temperature in the dark. The slices were rinsed three times with PBS and the nuclei were stained with DAPI (Beyotime, C1006) staining buffer for 15 min. A confocal microscope acquired fluorescent images.

2.14. Statistical analysis

Statistical analysis was done using Excel, Origin, and GraphPad Prism. Comparisons were made using a two-tailed, unpaired Student's *t*-test. $P < 0.05$ was considered statistically significant and all the results are expressed as mean ± s.d..

3. Results and discussion

The syntheses of CPT-SS-APBA prodrug is shown in Scheme 2. *2,4*-Dihydroxyacetophenone was selectively alkylated with *tert*-butyl bromoacetate to yield compound ***1*** in a 79% yield. The phenol group in

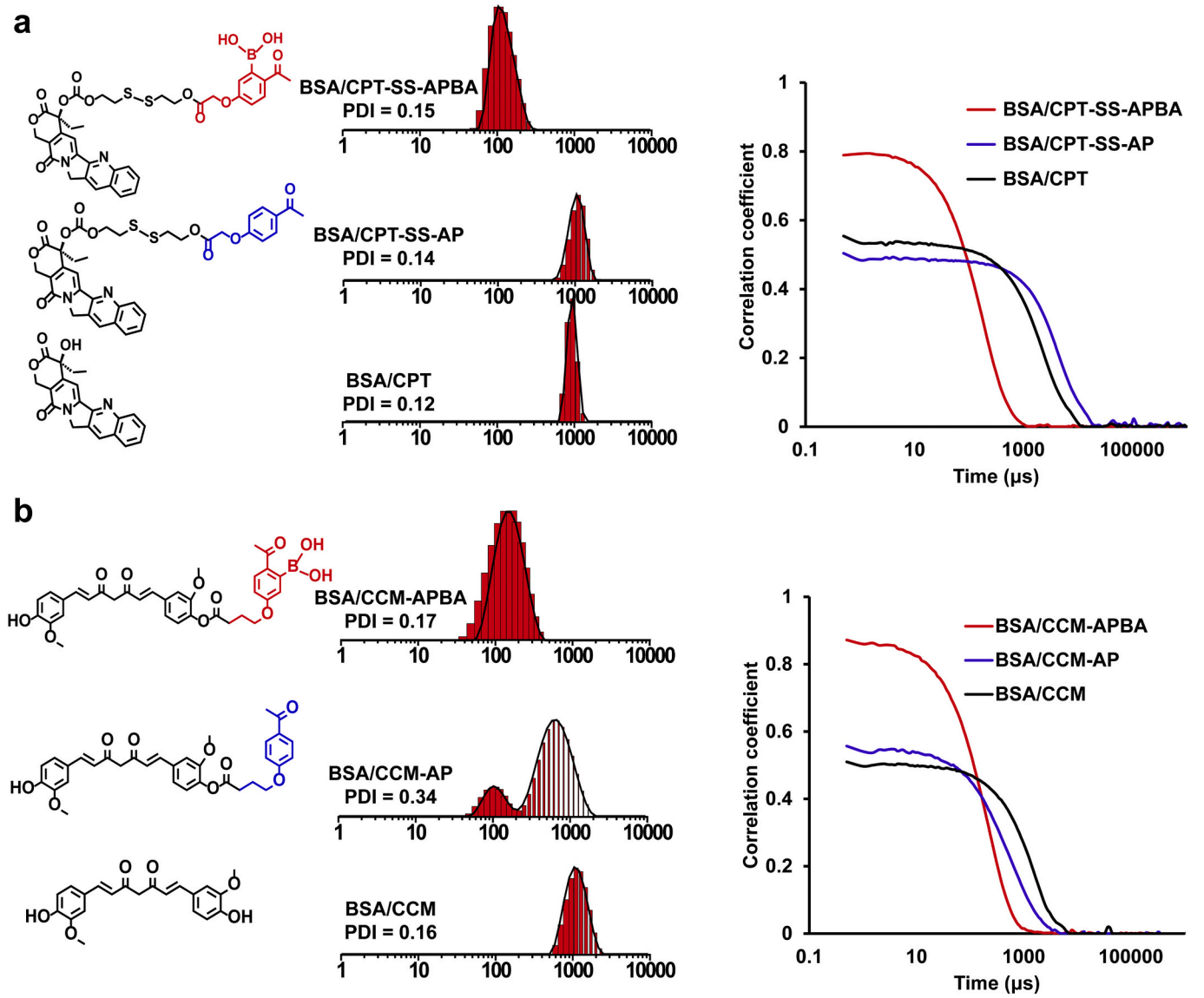

Fig. 1. 2-APBA-functionalized prodrugs complexing with albumin and forming nanoparticles. Particle size distributions (PSD in volume distribution, %) as obtained from DLS and correlation functions of the BSA solution (5 mg/mL) after adding the prodrugs or CPT or CCM control; the BSA/(pro)drug ratio was 5.0. (a) CPT or prodrugs; (b) CCM or prodrugs.

compound ***1*** was converted to a triflate (compound ***2***) in an alkaline environment, followed by a typical Miyaura borylation reaction with bis (pinocolato)diboron to afford compound ***3*** as a white solid. The disulfide linker was connected to CPT as reported [27] and subsequently conjugated with compound ***4*** to obtain compound ***6***. The pinacol group was then removed by boronic acid resin to produce CPT-SS-APBA. Similarly, the control prodrug with acetylphenyl (AP) group, CPT-SS-AP, was synthesized using the 4′-hydroxyacetophenone as the starting materials (Scheme 2i). The curcumin prodrugs, CCM-APBA and CCM-AP, were prepared similarly except using *tert*-butyl 4-bromobutanoate to avoid the steric hindrance (Scheme 2ii).

The resulting compounds were characterized and confirmed by ^{1}H NMR, ^{13}C NMR spectra, and ESI-MS spectra (Fig. S1–S17). It should be pointed out that in mass spectrometry under electrospray ionization conditions, arylboronic acids show unique properties due to the special gas-phase chemistry of boronic acid [28]. The CPT-SS-APBA and CCM-APBA peaks appeared as $[M+28+Na]^{+}$ because the boronic acid reacted with methanol to give the boronate esters (Fig. S10 & S15).

Once a hydrophobic drug is added to the BSA solution, drug molecules competitively assemble with themselves forming precipitation [29] or BSA forming adducts. The planar structures of CPT and CPT-SS-AP made them easily crystallize rather than assemble with BSA. As a result, adding CPT or control prodrug CPT-SS-AP to the BSA solution immediately produced large precipitates (Fig. 1a), giving very low drug loading contents (< 1%) and drug loading efficiency (< 10%) in BSA (Table S1). In contrast, the CPT-SS-APBA bound to BSA *via* forming iminoboronates and thus produced more hydrophobic CPT-SS-APBA/BSA adducts, which self-assembled adduct nanoparticles. Therefore, adding CPT-SS-APBA into the BSA solution with stirring gave a clear blueish solution. DLS measurements showed that the solution contained nanoparticles with sizes of ~100 nm (Fig. 1a). The CPT-equivalent (CPT-eq.)-loading contents could be controlled in a range of 2.20% to 9.55% (wt%) by tuning the BSA/CPT-SS-APBA ratios (Fig. S18, Table S2). The loading efficiencies were over 98% at the BSA to CPT-SS-APBA (*w*/w) ratios higher than 5.0 (Table S2). Very interestingly, the formed nanoparticle sizes were independent of the ratios, all about 125 nm (Table S2). BSA/CPT-SS-APBA at a ratio of 5.0 produced nanoparticles with a 7.68% CPT-eq.-loading content and a drug loading efficiency of 98.76% and was selected for further evaluations.

Similarly, CCM-APBA complexed with the BSA and produced

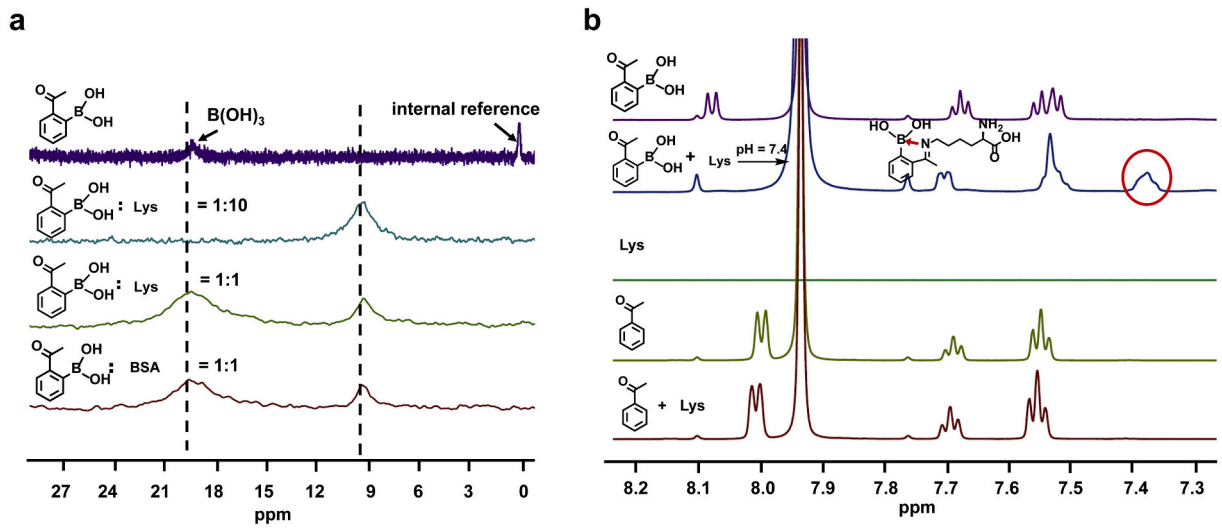

Fig. 2. Iminoboronate formation detected by ^{11}B NMR and ^{1}H NMR spectra. (a) ^{11}B NMR spectra of 2-APBA, and its mixture with lysine at the molar ratios of 1: 10 or 1:1 or with BSA at an equimolar ratio of BSA's primary amines in deuterated PBS buffer (pH = 7.4) calibrated against the BF_3 Et_2O (0 ppm). (b) ^{1}H NMR spectra of 2-APBA, its mixture with lysine (1:10), lysine, acetophenone, and acetophenone mixture with lysine (1:10).

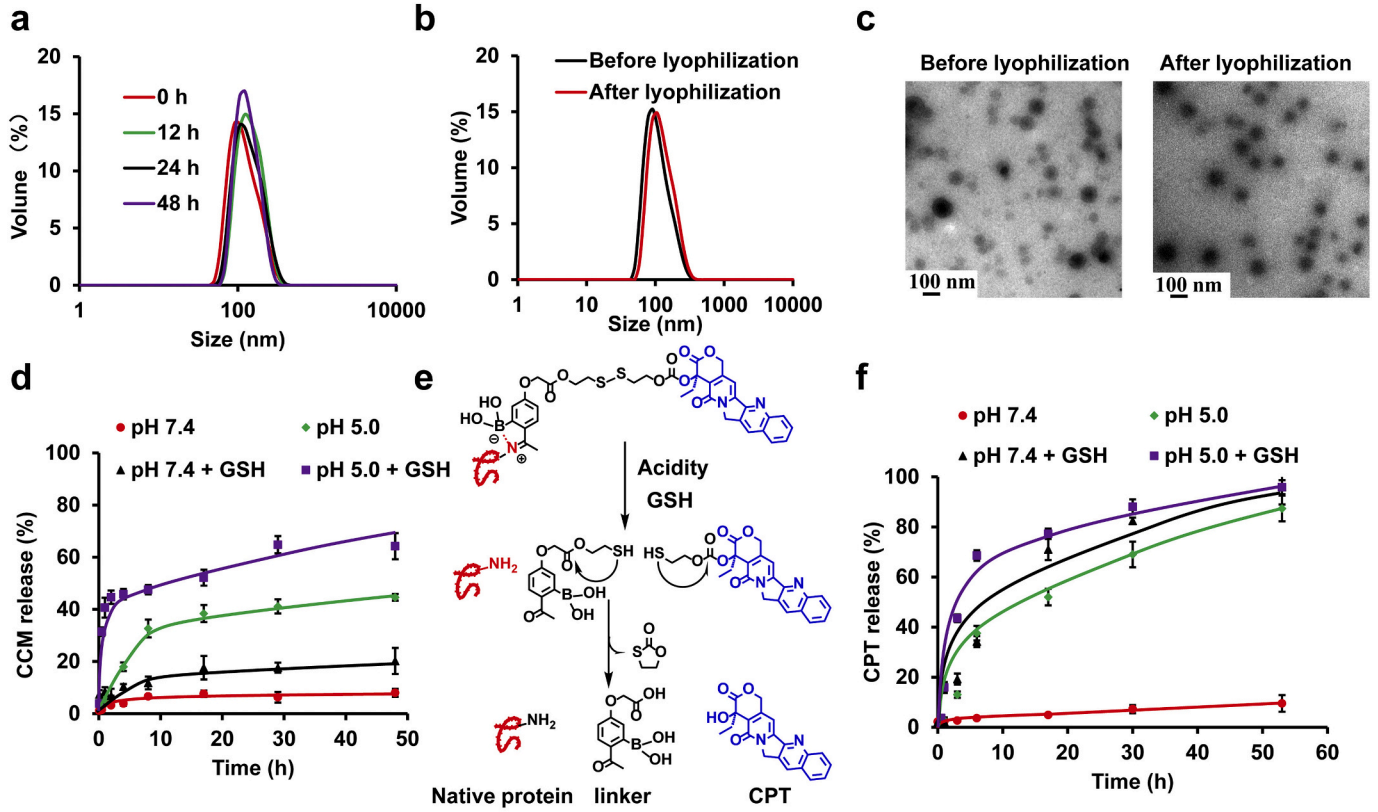

Fig. 3. Stability and drug release of the BSA/prodrug nanoparticles. (a) The DLS patterns of BSA/CPT-SS-APBA nanoparticles in the cell growth medium with 10% FBS for different times. (b,c) The lyophilization effects: the DLS patterns (b) and representative TEM images (c) of BSA/CPT-SS-APBA nanoparticles before and after lyophilization. (d) The release kinetic of CCM from BSA/CCM-APBA nanoparticles with or without GSH (10 mM) at pH 7.4 and 5.0. (e) Scheme of CPT-release from BSA/CPT-SS-APBA nanoparticles in response to GSH and acidity. (f) The release kinetics of CPT from BSA/CPT-SS-APBA nanoparticles with or without GSH (10 mM) at pH 7.4 and 5.0.

nanoparticles of sizes about 130 nm, whereas adding CCM or CCM-AP into the BSA solution also precipitated (Fig. 1b). These results indicated that 2-APBA-modified prodrugs efficiently complexed with BSA, forming BSA-drug adducts that self-assembled into ~100 nm NPs.

The 2-APBA-functionalized prodrugs could also bind other proteins, such as RNase A, IgG, and aPD1. CPT-SS-APBA or CCM-APBA-bound proteins self-assembled into nanoparticles (Fig. S19-S21 and Table S1). Interestingly, CPT-SS-APBA could also form uniform nanoparticles once adding in mouse serum, indicating that they bound the BSA in the serum (Fig. S22).

The iminoboronate formation between the prodrug and BSA's primary amines was detected using 2-APBA and lysine as the model

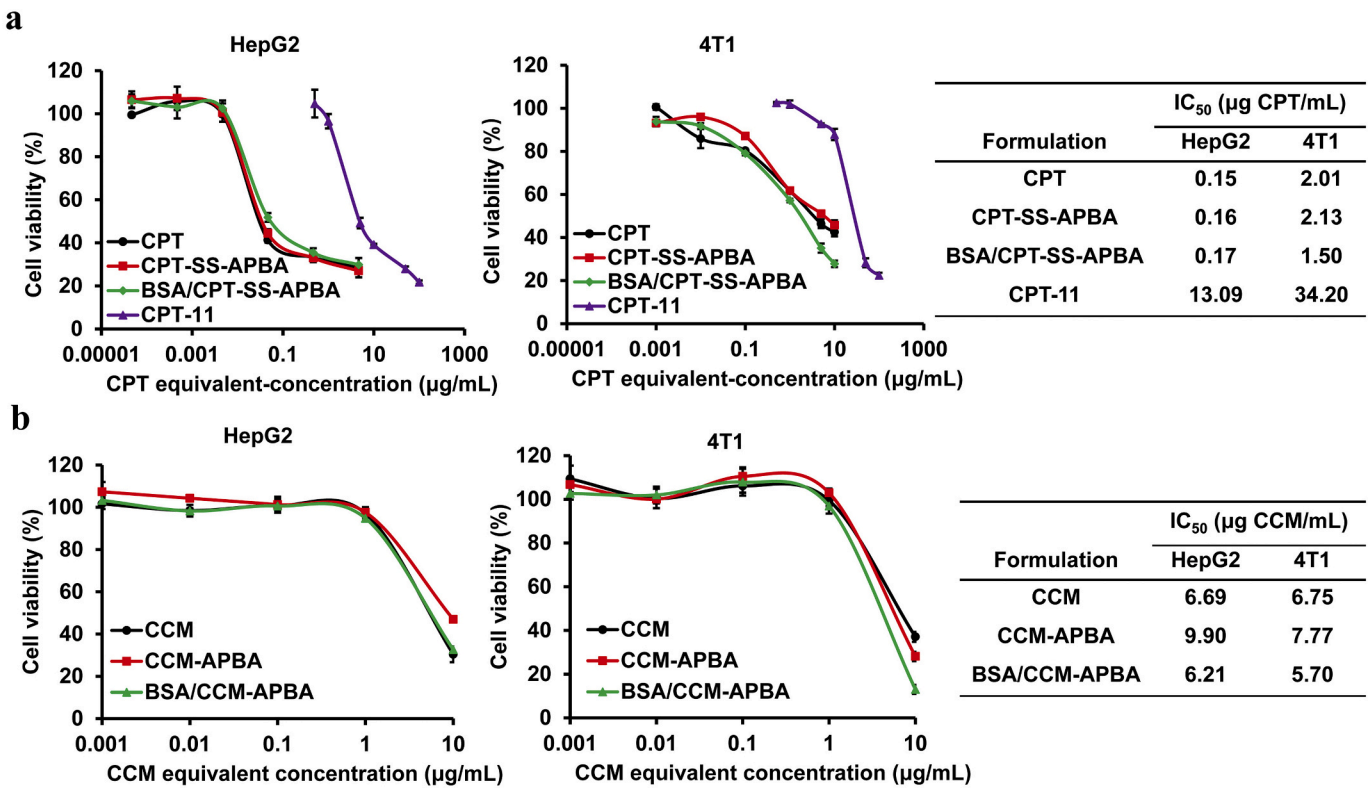

Formulation	IC_{50} (μg CPT/mL) HepG2	4T1
CPT	0.15	2.01
CPT-SS-APBA	0.16	2.13
BSA/CPT-SS-APBA	0.17	1.50
CPT-11	13.09	34.20

Formulation	IC_{50} (μg CCM/mL) HepG2	4T1
CCM	6.69	6.75
CCM-APBA	9.90	7.77
BSA/CCM-APBA	6.21	5.70

Fig. 4. Cytotoxicity assays. (a) The MTT assay curves of free CPT, CPT-SS-APBA, BSA/CPT-SS-APBA, and CPT-11 against HepG2 and 4 T1 cells and their IC_{50} values. (b) The MTT assay curves of free CCM, BSA/CCM-APBA, and CCM-APBA against HepG2 and 4T1cells and their calculated IC_{50} values; 48 h incubation; $n = 3$.

compounds with ^{11}B NMR and ^{1}H NMR in deuterated PBS (Fig. 2**).** 2-APBA alone had a typical peak of aryl boronic acid/ester at 18–20 ppm ($BF_3{\cdot}Et_2O$ as the internal reference). Mixing 2-APBA with lysine produced a new peak at 8–10 ppm, which is characteristic of the anionic boron in iminoboronates [30]. The peak also appeared when 2-APBA was mixed with BSA at an equimolar ratio of BSA's primary amines, indicating the formation of iminoboromates, as further verified by the ^{1}H NMR spectra (Fig. 2b**)**. In contrast, acetophenone did not react with the Lys amines.

The serum stability and lyophilization of the BSA/CPT-SS-APBA nanoparticles were further investigated. As depicted in Fig. 3a and Fig. S23, both the size (in the presence of 10% FBS) and zeta potential (in the presence of 100% mouse plasma) of the BSA/CPT-SS-APBA maintained constant over 48 h, indicating great colloidal stability of the nanoparticles. After lyophilization, the reconstructed BSA/CPT-SS-APBA and BSA/CCM-APBA nanoparticles maintained the same sizes and zeta-potentials (Fig. 3b, Fig. S24), which were further verified by the TEM results (Fig. 3c, Fig. S25).

The drug release profiles of the formed nanoparticles were first evaluated using BSA/CCM-APBA nanoparticles. BSA/CCM-APBA nanoparticles were stable and free of burst release; only ~5% CCM was released after 48 h at the physiological pH. GSH triggered the hydrolysis of the iminoboronate by disrupting the B-N bond, but the hydrolysis of CCM-APBA to CCM at physiological pH was slow and enhanced at pH 5.0 (Fig. 3d). However, the hydrolysis of CCM-APBA was incomplete, only ~60%, even after 48 h incubation at pH 5.0 with GSH. In this regard, the disulfide linker was introduced into the CPT-SS-APBA prodrug to accelerate the prodrug's conversion to CPT by responding to the intracellular glutathione (Fig. 3e). Indeed, once adding GSH to the solution of BSA/CPT-SS-APBA at pH 7.4 or 5.0, micrometer-sized precipitates were observed, and the original 100 nm peak disappeared (Fig. S26), indicating complete disassembly of the nanoparticles and the

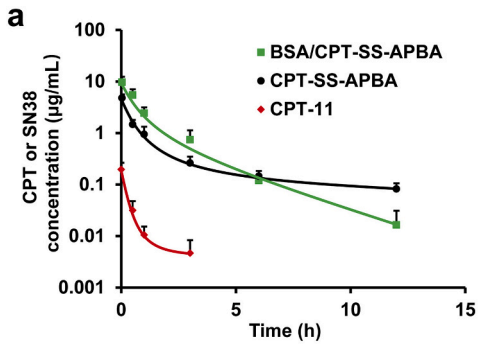

b

Parameter	BSA/CPT-SS-APBA	CPT-SS-APBA	CPT-11
$T_{1/2}$ alpha (h)	0.45	0.13	0.15
$T_{1/2}$ beta (h)	2.74	1.28	1.97
$AUC_{0\text{-}t}$ (μg/mL*h)	10.56	4.28	0.11
MRT (h)	1.29	2.21	0.71
CL (L/h/kg)	0.43	1.05	93.89

Fig. 5. Pharmacokinetic profiles and parameters of CPT-11, free CPT-SS-APBA, and BSA/CPT-SS-APBA nanoparticles. (a) Blood clearance profiles and (b) pharmacokinetic parameters of CPT-11, free CPT-SS-APBA, and BSA/CPT-SS-APBA nanoparticles at a CPT (or SN38)-eq. dose of 5 mg/kg. $T_{1/2}$ alpha: half-life time of distribution phase. $T_{1/2}$ beta: half-life time of elimination phases. $AUC_{0\text{-}t}$: area under the curve. MRT: mean residence time. CL: clearance. Data are depicted as mean ± SD.

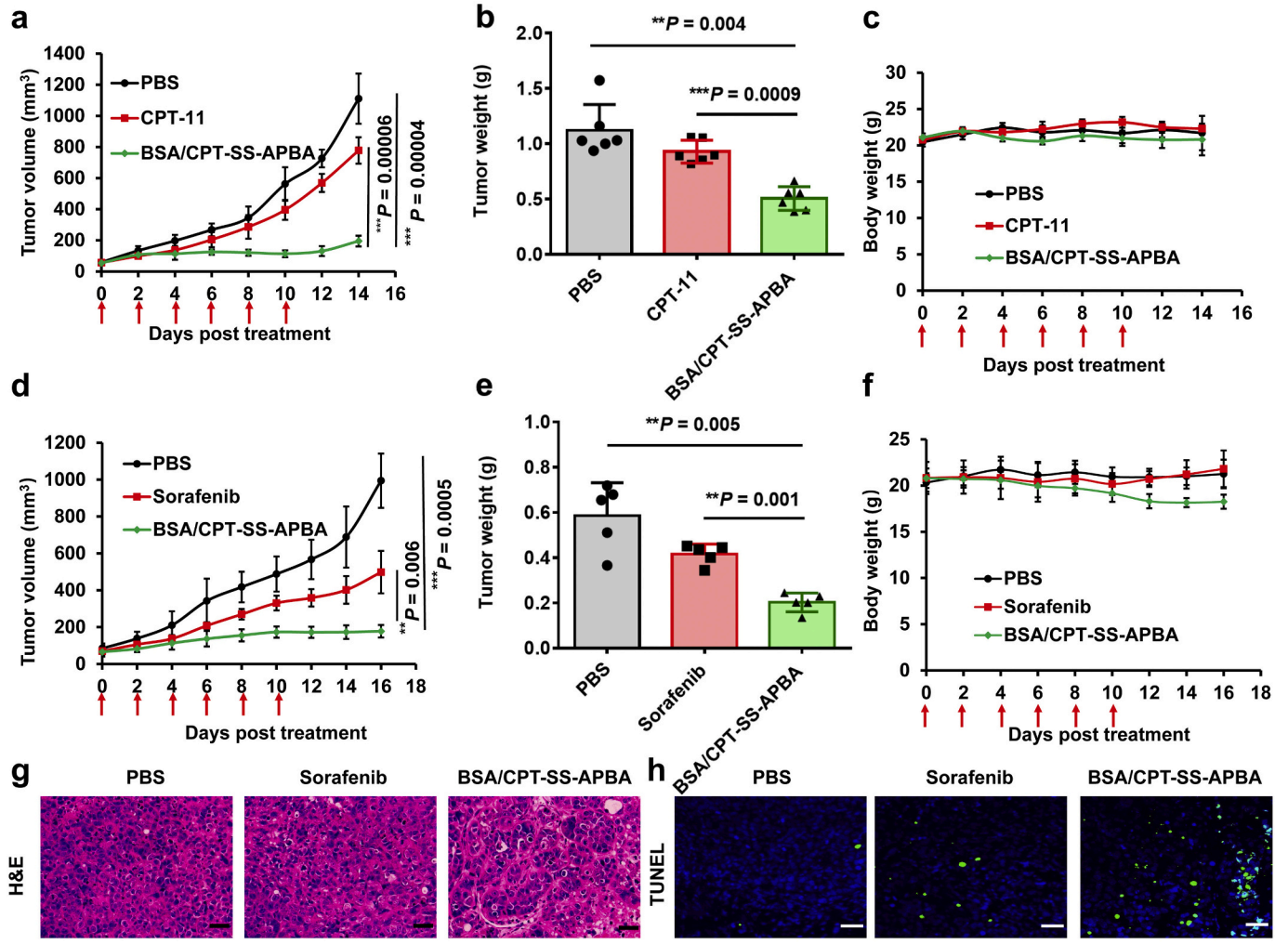

Fig. 6. *In vivo* antitumor activity assays of BSA/CPT-SS-APBA nanoparticles. (a–c) The BALB/c mice bearing subcutaneous 4 T1 tumors ($n = 6$) were intravenously treated with PBS, CPT-11 (5 mg/kg) and BSA/CPT-SS-APBA nanoparticles (CPT-eq. dose 5 mg/kg); (d–f) The BALB/c nude mice bearing subcutaneous HepG2 tumors ($n = 5$) were treated with PBS, sorafenib (oral administration, 10 mg/kg) and BSA/CPT-SS-APBA (*i.v.*, CPT-eq. dose 5 mg/kg). Dosing schedules are indicated by red arrows. (a,d) Tumor volumes as a function of time. (b,e) The average tumor weight of each group at the end of the antitumor experiment. (c,f) Body weights change of the mice during the treatment. (g,h) Representative histological features (g) and TUNEL immunofluorescence staining (h) of sections of the subcutaneous HepG2 tumor resected after the mice were sacrificed. Scale bars = 40 μm. Error bars represent the standard deviation of means; Statistical significance: *P* values were obtained using the Student's *t*-test. $^{*}P < 0.05$, $^{**}P < 0.01$, $^{***}P < 0.001$. (For interpretation of the references to colour in this figure legend, the reader is referred to the web version of this article.)

precipitation of CPT. The CPT-release from BSA/CPT-SS-APBA nanoparticles was monitored by a dialysis method (Fig. 3f). BSA/CPT-SS-APBA nanoparticles were very stable; less than 10% CPT was released after 48 h incubation in PBS at the physiological pH. Both the GSH and acidity dramatically accelerated the CPT release from the particles. The CPT- release rate was further accelerated at pH 5.0 in the presence of GSH. Thus, the BSA/CPT-SS-APBA nanoparticles would keep stable in the bloodstream while selectively release CPT in the acidic lysosomes and the tumor cell cytosol rich in GSH.

The *in vitro* cytotoxicity of BSA/CPT-SS-APBA nanoparticles against HepG2 and 4 T1 cells was determined by the MTT assay (Fig. 4a). CPT-SS-APBA, BSA/CPT-SS-APBA, CPT-11, and free CPT all showed dose-dependent cytotoxicity against both cell lines. The IC_{50} values of BSA/CPT-SS-APBA against HepG2 and 4 T1 cells were 0.17 and 1.50 μg/mL, respectively, comparable to those of free CPT and CPT-SS-APBA, indicating efficient CPT-release from the nanoparticles in the cytoplasm. In contrast, the IC_{50} values of CPT-11 were higher than 10 μg/mL to the cells due to the low conversation rate of CPT-11 [31]. Similarly, CCM, CCM-APBA, and BSA/CCM-APBA nanoparticles showed similar cytotoxicity against HepG2 and 4 T1 cells, further suggesting the CCM-APBA can be effectively released from the nanoparticles upon internalized by the tumor cells (Fig. 4b).

The pharmacokinetics of BSA/CPT-SS-APBA nanoparticles was subsequently estimated, and the small molecular drug CPT-11 was used as control. Not surprisingly, CPT-11 was quickly cleared, and the plasma concentrations of SN38 were below 0.1 μg/mL in minutes. The BSA/CPT-SS-APBA underwent a slower clearance. The serum CPT level in the mice treated with BSA/CPT-SS-APBA nanoparticles was still approximately 0.1 μg/mL after 6 h. Thus, the BSA/CPT-SS-APBA nanoparticles had an AUC ~96 fold larger than CPT-11 (Fig. 5a–b). Therefore, the BSA/CPT-SS-APBA nanoparticles could accumulate in the tumor tissue through the passive enhanced permeability and retention (EPR) [32] effect. Notably, CPT-SS-APBA also had much better pharmacokinetics than CPT-11 because it could rapidly bind to the endogenous serum proteins. However, the severe acute side effect was observed when free CPT-SS-APBA was *i.v.* injected because of its hydrophobic nature of CPT-SS-APBA and uncontrolled binding to key proteins. The biodistribution of BSA/CPT-SS-APBA was conducted on the subcutaneous 4 T1 xenograft tumor model (Fig. S27). BSA/CPT-SS-APBA had very low levels in the heart, spleen, and lung. Notably, BSA/

CPT-SS-APBA accumulated significantly more in the kidney, liver, and tumors. These biodistribution profiles indicate an effective tumor-targeting capability of BSA/CPT-SS-APBA.

Encouraged by the excellent *in vitro* cytotoxicity and the improved pharmacokinetics, BSA/CPT-SS-APBA nanoparticles were assessed for tumor therapy in a 4 T1 tumor-bearing xenograft model with CPT-11 as control (Fig. 6a). BSA/CPT-SS-APBA nanoparticles exhibited improved antitumor effects and delayed tumor progression compared with PBS ($P = 0.00004$) and CPT-11 ($P = 0.00006$). The tumor inhibition rate calculated from the tumor weight was 55.5% for BSA/CPT-SS-APBA nanoparticles compared with 29.1% for CPT-11 (Fig. 6b). No significant body weight loss was observed during the treatment period (Fig. 6c).

The BSA/CPT-SS-APBA against the subcutaneous HepG2 tumor model was further evaluated and compared with a clinical used anti-hepatoma drug sorafenib (Fig. 6d-f). The BSA/CPT-SS-APBA nanoparticles again showed an enhanced tumor inhibition activity compared to PBS ($P = 0.0005$) and sorafenib ($P = 0.006$) with a higher tumor inhibition rate than sorafenib (65.5% *vs* 29.1%, $P = 0.001$). The body weights of the mice treated with BSA/CPT-SS-APBA nanoparticles decreased slightly during the treatment but remained stable once the treatment was terminated (Fig. 6f). The hematoxylin and eosin (H & E) staining showed no obvious organ toxicity after BSA/CPT-SS-APBA nanoparticle treatment (Fig. S28). The H&E staining of the tumors showed extensive tumor cell vacuolization and nuclear condensation in the BSA/CPT-SS-APBA treated tumors compared to the tightly-packed tumor cells in the PBS and sorafenib treated group, suggesting that BSA/CPT-SS-APBA induced remarkable cell apoptosis. The TUNEL immunofluorescence assays also verified these results (Fig. 6g,h).

4. Conclusion

In summary, 2-acetylphenylboronic acid-functionalized CPT and CCM prodrugs can efficiently bind proteins by forming iminoboronates with lysine ε-amines and induce the protein-drug conjugates self-assemble into nanoparticles with high loading efficiency and improved colloidal stability. The acidity or GSH-labile iminoboronates renders the burst-free nanoparticles fast-drug release. As a result, BSA/CPT-SS-APBA nanoparticles showed enhanced anticancer efficacy in subcutaneous 4 T1 and HepG2 tumor models than clinical used CPT-11 and sorafenib. Therefore, this work demonstrates a versatile protein-binding prodrug platform applicable for protein-based drug formulations and even antibody-drug conjugates.

Declaration of Competing Interest

All the authors declare no conflicting interests.

Acknowledgment

We thank the National Natural Science Foundation of China (51833008, 21704090, 51522304), the National Key Research and Development Program (2016YFA0200301), and the China postdoctoral Science Foundation (NO. 2019M662059) for financial support.

Appendix A. Supplementary data

Supplementary data to this article can be found online at https://doi.org/10.1016/j.jconrel.2020.12.035.

References

[1] Z. Liu, X. Chen, Simple bioconjugate chemistry serves great clinical advances: albumin as a versatile platform for diagnosis and precision therapy, Chem. Soc. Rev. 45 (2016) 1432–1456.
[2] A.O. Elzoghby, W.M. Samy, N.A. Elgindy, Albumin-based nanoparticles as potential controlled release drug delivery systems, J. Control. Release 157 (2012) 168–182.
[3] F. Kratz, A clinical update of using albumin as a drug vehicle - a commentary, J. Control. Release 190 (2014) 331–336.
[4] F.F. An, X.H. Zhang, Strategies for preparing albumin-based nanoparticles for multifunctional bioimaging and drug delivery, Theranostics 7 (2017) 3667–3689.
[5] Q. Chen, C. Liang, C. Wang, Z. Liu, An imagable and photothermal "Abraxane-like" nanodrug for combination cancer therapy to treat subcutaneous and metastatic breast tumors, Adv. Mater. 27 (2015) 903–910.
[6] T.H. Kim, H.H. Jiang, Y.S. Youn, C.W. Park, K.K. Tak, S. Lee, H. Kim, S. Jon, X. Chen, K.C. Lee, Preparation and characterization of water-soluble albumin-bound curcumin nanoparticles with improved antitumor activity, Int. J. Pharm. 403 (2011) 285–291.
[7] B. Elsadek, F. Kratz, Impact of albumin on drug delivery–new applications on the horizon, J. Control. Release 157 (2012) 4–28.
[8] Y. Min, J.M. Caster, M.J. Eblan, A.Z. Wang, Clinical translation of nanomedicine, Chem. Rev. 115 (2015) 11147–11190.
[9] A.M. Sofias, M. Dunne, G. Storm, C. Allen, The battle of "nano" paclitaxel, Adv. Drug Deliv. Rev. 122 (2017) 20–30.
[10] E. Bernabeu, M. Cagel, E. Lagomarsino, M. Moretton, D.A. Chiappetta, Paclitaxel: what has been done and the challenges remain ahead, Int. J. Pharm. 526 (2017) 474–495.
[11] S. Hu, E. Lee, C. Wang, J. Wang, Z. Zhou, Y. Li, X. Li, J. Tang, D.H. Lee, X. Liu, Y. Shen, Amphiphilic drugs as surfactants to fabricate excipient-free stable nanodispersions of hydrophobic drugs for cancer chemotherapy, J. Control. Release 220 (2015) 175–179.
[12] X. Yang, X. Xue, Y. Luo, T.Y. Lin, H. Zhang, D. Lac, K. Xiao, Y. He, B. Jia, K.S. Lam, Y. Li, Sub-100nm, long tumor retention SN-38-loaded photonic micelles for tri-modal cancer therapy, J. Control. Release 261 (2017) 297–306.
[13] W. Um, J. Park, A. Youn, H. Cho, S. Lim, J.W. Lee, H.Y. Yoon, D.K. Lim, J.H. Park, K. Kim, A comparative study on albumin-binding molecules for targeted tumor delivery through covalent and noncovalent approach, Bioconjug. Chem. 30 (2019) 3107–3118.
[14] D. Pilati, K.A. Howard, Albumin-based drug designs for pharmacokinetic modulation, Expert Opin. Drug Metab. Toxicol. 16 (2020) 783–795.
[15] J. Delahousse, C. Skarbek, A. Paci, Prodrugs as drug delivery system in oncology, Cancer Chemother. Pharmacol. 84 (2019) 937–958.
[16] X. Liu, R.P. Mohanty, E.Y. Maier, X. Peng, S. Wulfe, A.P. Looney, K.L. Aung, D. Ghosh, Controlled loading of albumin-drug conjugates ex vivo for enhanced drug delivery and antitumor efficacy, J. Control. Release 328 (2020) 1–12.
[17] F. Kratz, G. Ehing, H.M. Kauffmann, C. Unger, Acute and repeat-dose toxicity studies of the (6-maleimidocaproyl)hydrazone derivative of doxorubicin (DOXO-EMCH), an albuminbinding prodrug of the anticancer agent doxorubicin, Hum. Exp. Toxicol. 26 (2007) 19–35.
[18] D. Lebrecht, A. Geist, U.P. Ketelsen, J. Haberstroh, B. Setzer, F. Kratz, U.A. Walker, The 6-maleimidocaproyl hydrazone derivative of doxorubicin (DOXO-EMCH) is superior to free doxorubicin with respect to cardiotoxicity and mitochondrial damage, Int. J. Cancer 120 (2007) 927–934.
[19] B. Akgun, D.G. Hall, Boronic acids as bioorthogonal probes for site-selective labeling of proteins, Angew. Chem. Int. Ed. Engl. 57 (2018) 13028–13044.
[20] S. Cambray, J. Gao, Versatile bioconjugation chemistries of ortho-boronyl aryl ketones and aldehydes, Acc. Chem. Res. 51 (2018) 2198–2206.
[21] H. Faustino, M. Silva, L.F. Veiros, G.J.L. Bernardes, P.M.P. Gois, Iminoboronates are efficient intermediates for selective, rapid and reversible N-terminal cysteine functionalisation, Chem. Sci. 7 (2016) 5052–5058.
[22] P.M. Cal, J.B. Vicente, E. Pires, A.V. Coelho, L.F. Veiros, C. Cordeiro, P.M. Gois, Iminoboronates: a new strategy for reversible protein modification, J. Am. Chem. Soc. 134 (2012) 10299–10305.
[23] R. Ma, C. Zhang, Y. Liu, C. Li, Y. Xu, B. Li, Y. Zhang, Y. An, L. Shi, Iminoboronate-based dual-responsive micelles via subcomponent self-assembly for hydrophilic 1,2-diol-containing drug delivery, RSC Adv. 7 (2017) 21328–21335.
[24] A. Bandyopadhyay, J. Gao, Iminoboronate-based peptide cyclization that responds to pH, oxidation, and small molecule modulators, J. Am. Chem. Soc. 138 (2016) 2098–2101.
[25] P. Cal, R.F.M. Frade, C. Cordeiro, P.M.P. Gois, Reversible lysine modification on proteins by using functionalized boronic acids, Chem-Eur. J. 21 (2015) 8182–8187.
[26] P.M. Cal, R.F. Frade, V. Chudasama, C. Cordeiro, S. Caddick, P.M. Gois, Targeting cancer cells with folic acid-iminoboronate fluorescent conjugates, Chem. Commun. 50 (2014) 5261–5263.
[27] Q. Zhou, S.Q. Shao, J.Q. Wang, C.H. Xu, J.J. Xiang, Y. Piao, Z.X. Zhou, Q.S. Yu, J. B. Tang, X.R. Liu, Z.H. Gan, R. Mo, Z. Gu, Y.Q. Shen, Enzyme-activatable polymer-drug conjugate augments tumour penetration and treatment efficacy, Nat. Nanotech. 14 (2019) 799–809.
[28] L.F. Wang, C.F. Dai, S.K. Burroughs, S.M.L. Wang, B.H. Wang, Arylboronic acid chemistry under electrospray conditions, Chem-Eur. J. 19 (2013) 7587–7594.
[29] S.X. Lv, Y.C. Wu, K.M. Cai, H. He, Y.J. Li, M. Lan, X.S. Chen, J.J. Cheng, L.C. Yin, High drug loading and sub-quantitative loading efficiency of polymeric micelles driven by donor-receptor coordination interactions, J. Am. Chem. Soc. 140 (2018) 1235–1238.

[30] A. Bandyopadhyay, J.M. Gao, Iminoboronate formation leads to fast and reversible conjugation chemistry of alpha-nucleophiles at neutral pH, Chem-Eur. J. 21 (2015) 14748–14752.

[31] P.D. Senter, K.S. Beam, B. Mixan, A.F. Wahl, Identification and activities of human carboxylesterases for the activation of CPT-11, a clinically approved anticancer drug, Bioconjug. Chem. 12 (2001) 1074–1080.

[32] J. Shi, P.W. Kantoff, R. Wooster, O.C. Farokhzad, Cancer nanomedicine: progress, challenges and opportunities, Nat. Rev. Cancer 17 (2017) 20–37.